Supporting Information

Vandecasteele et al. 10.1073/pnas.1411233111

SI Methods

Animals. A total of 26 adult mice (2–7 mo) of both sexes were used in this study. Three transgenic mouse strains were used: 14 mice expressing the Cre-recombinase under the control of the choline acetyl-transferase promoter (ChAT-Cre, Jackson Labs strain 006410, or GENSAT GM60) were injected with Cre-dependent Channelrhodopsin2 (ChR2) or control viral vector (discussed below), whereas 9 mice were the offspring of the ChAT-Cre line crossed with the Ai32 reporter line carrying a Cre-dependent, enhanced YFP (EYFP)-tagged ChR2(H134R)-containing expression cassette (Allen Institute for Brain Research, or Jackson Labs, strain 12569). Three mice were offspring of ChAT-Cre mice crossed with Cre-reporter line Ai27, bearing a Cre-dependent ChR2(H134R)-tdTomato construct (Allen Institute) (see ref. 1 for details about Ai32 and Ai27 mouse strains). All experiments were performed in accordance with the National Institutes of Health *Guide for the Care and Use of Laboratory Animals*, the Institutional Ethical Codex, Hungarian Act of Animal Care and Experimentation (1998, XXVIII, section 243/1998), and the European Union guidelines (directive 2010/63/EU), and with the approval of the Institutional Animal Care and Use Committees at Rutgers University, New York University, the Institute for Experimental Medicine of the Hungarian Academy of Science, and the Center for Interdisciplinary Research in Biology. All mice were housed in 12:12 light/dark cycle. Water and food were available for ad libitum consumption. All efforts were made to minimize pain and suffering and to reduce the number of animals used.

Surgery. General anesthesia was induced with isoflurane inhalation. For acute recordings, anesthesia was maintained with urethane injection (1–1.5 mg/kg, i.p. initial injection, supplemented if necessary up to 2.2 mg/kg). For survival surgery (injection of virus, or implantation of probes and optic fibers), anesthesia was maintained with one i.p. injection of ketamine–xylazine (120 mg/kg and 16 mg/kg, respectively), followed by isoflurane inhalation delivered through a mask mounted on the stereotaxic apparatus. Body temperature was kept constant with a heating pad.

Virus injection. The surgeries were performed inside an isolation cabinet under biosafety level-2 (BSL-2) confinement or in a BSL-2 virus injection facility. Briefly, the skull was exposed under antiseptic conditions using local anesthesia with bupivacaine/lidocaine and a hole was drilled above the medial septum (MS) [anteroposterior (AP) +0.98 mm from bregma, mediolateral (ML) +0.9 mm, 14° angle insertion, or AP +0.8 mm, ML +0.7mm, 10° angle insertion or AP +0.7–0.9 mm, midline insertion at 0° angle]. A glass pipette (30- to 50-μm tip) connected to a Nanoject II/Nanoliter 2000 microinjector (Drummond Scientific Co. or WPI Inc.), or alternatively, a cannula connected to a 10-μL Hamilton syringe was used to inject 0.05–0.7 μL of virus solution at one to five different depths between 3.8 and 4.6 mm (14° angle insertion) or between 2.8 and 4 mm (10° angle insertion), or at 3.0–3.4 mm (midline, 0° insertion), over 10–30 min. After injection the pipette was removed slowly (0.1 then 0.5-mm steps, 10-min waiting periods between each), the scalp was sutured, and injected mice were housed in BSL-2 quarantine for 2–4 wk before experimentation.

Acute and chronic implantations. The scalp was shaved after local anesthesia with bupivacaine/lidocaine and the skull was exposed in antiseptic conditions. Stereotaxic locations of the MS (AP +0.8 mm, ML +0.7 mm and 10° angle, or ML 0 mm and 0° angle insertion) and hippocampus (AP −1.7 to −2.5 mm from bregma, ML −1 to −2 mm) were marked on the skull. Two holes were drilled over the cerebellum to insert the ground and reference miniature screws. Craniotomies were performed at marked locations, and dura was gently removed. After implantation of probes and optic fibers (discussed below), a paraffin–wax mixture was used to seal the craniotomies. For chronic implantations, extra steps were performed: One or two extra support screws were inserted in opposite skull plates and implants were secured to the skull using dental cement encompassing all screws, and protected by a grounded copper mesh. Appropriate suture and postoperative care of the wounds was ensured, and recordings began after 1 wk of recovery (see ref. 2 for detailed procedures of chronic surgery and recordings in rats).

Viral Constructs. Two adeno-associated viruses (AAV) were used, one bearing ChR-2 with a YFP reporter and a control virus bearing only the YFP reporter. Both viruses are based on the same double-floxed inverse ORF technology designed by Karl Desseiroth (Stanford University, Stanford, CA) and used with his permission (www.stanford.edu/group/dlab/optogenetics/sequence_info.html#dio): The ChR-2 virus EF1a.DIO.hChR2(H134R)-EYFP.WPRE.hGH construct was packaged into AAV serotypes 2, produced at Vector Biolabs and a gift from Tibor Koos (Center for Molecular and Behavioral Neuroscience, Rutgers University, Newark, NJ), or serotype 5, purchased form Penn Vector Core. The control virus, EF1a.DIO.EYFP.WPRE.hGH (27056; Addgene), was packaged into AAV serotype 1, bought from Penn Vector Core, a gift from Marco Diana (Institut de Biologie de l'Ecole Normale Supérieure, Paris), and diluted three times in sterile PBS before use.

Silicon Probes and Optic Fiber Implants. In the hippocampus, linear multichannel silicon probes (16 or 32 sites, 50- or 100-μm spacing; NeuroNexus) were inserted across the CA1–DG axis, at a 2.1- to 2.5-mm depth in 17 animals. In three animals, 16-site tetrode-like probes (2 × 2 or 4 × 1 tetrode; NeuroNexus) were mounted on a microdrive (see ref. 2 for microdrive details), inserted above CA1 pyramidal layer (1-mm depth) and progressively lowered during recovery down to the pyramidal layer (recognized by the presence of ripples and stronger unit activity). Silicon probes were painted with 2% DiI solution (Sigma) to facilitate the ex vivo localization confirmation. In the MS, for optogenetic stimulation only (16 animals), 125-μm-diameter optic fibers with a 50- to 105-μm core (Thorlabs) were implanted at a 3.0- to 3.5-mm depth (depending on the stereotaxic angle chosen). Before surgery, the optic fibers were stripped from the buffer layer and connectorized with 1.25-mm ceramic ferrules (extracted from LC connectors; Thorlabs). A pencil-shaped tip was obtained by etching 30′ in hydrofluoric acid (Sigma) to facilitate the insertion in the brain. For recording entrained cells in the MS together with optogenetic stimulation (four animals), custom-made optrodes were used: 10- to 50-μm core optic fibers (Thorlabs) were stripped from buffer layer and progressively etched down to a 2- to 10-μm tip in hydrofluoric acid before being attached to 12- to 16-site tetrode-like silicon probes (NeuroNexus Tech) by UV light-curing epoxy (see refs. 3 and 4 for optrode construction details). Optrodes were lowered to 2.8 mm and then progressively until typical MS activity was encountered in response to tail pinch [local field potentials (LFP) theta rhythm, presence of theta-on or theta-burst unit activity].

Optogenetic Stimulation. Light from a 473-nm diode-pumped solid-state (DPSS) laser (Dreamlasers) was collimated with a fiberport (Thorlabs) or delivered by a 475-nm laser diode light

source (FLS-475 nm–20 mW; DIPSI) into a custom patch cord (Thorlabs) connected to the brain-implanted optic fiber. Light intensity was driven by analog modulation of the DPSS power supply, using a Master-8 pulse stimulator (AMPI), a MATLAB-controlled DAQ-board (National Instruments or Measurement Computing Corp.), or a CED micro1401 mkII data acquisition system (Cambridge Electronic Devices) to generate square or sinusoidal pulses. For stimulation only of MS, maximum light intensity (crest of the sine wave, or plateau pulse amplitude) was adjusted using a photodiode power sensor coupled to a power meter (S130A and PM30 or S130C and PM100USB; Thorlabs), taking into account the patch cord-to-fiber coupling (measured before implantation of the fiber), to obtain a maximum of 5–10 mW at the tip of the fiber in the brain. For recording of entrained cells in MS using optrodes, owing to etching and diffraction of light by epoxy the maximum light at the tip of the fiber was <0.6 mW. Pulse trains consisted of 10- to 100-ms pulses delivered at various frequencies ranging between 0.5 and 20 Hz. During sine wave stimulation 0.5- to 12-Hz sinuses were delivered for 5–60 s.

Electrophysiological Recordings. Extracellular signal was amplified (20×) with a VLSI headstage (Plexon) and acquired continuously at 32.5 kHz using a multichannel DigiLynx system (Neuralynx) or amplified, multiplexed, and acquired continuously at 20 kHz using a multichannel KJE-1001 system (5) (Amplipex) and stored for offline analysis (discussed below). Twelve animals underwent urethane acute recordings only (4 for MS-cells entrainment and 3 mice for control stimulation). Five animals underwent chronic recordings only. Two animals underwent recordings during the chronic implantation (during isoflurane anesthesia), followed by freely moving chronic recordings. One animal underwent chronic recordings followed by urethane acute recordings. For chronic recording, after postoperative recovery animals were recorded in their home cage during sleep, alert immobility, or actively awake (grooming, sniffing, etc.) and/or during the exploration of a different environment (1-m × 7-cm linear track, baited with sucrose solution or water at each end, or a 60- × 60-cm open field arena). Before linear track sessions mice were water-deprived for 1 d. Speed was monitored by video tracking coupled to the recording system.

Histological Processing. To confirm probe track location, animals were perfused transcardially under deep anesthesia with saline followed by fixative [4% (wt/vol) paraformaldehyde (PFA) or 10% (vol/vol) formaline solution]. Brain was removed and postfixed overnight in fixative then rinsed in PBS and cut to 60- to 80-μm-thick coronal slices using a vibratome (VT1200; Leica). Slices were mounted in VectaShield (Vector Laboratories) to confirm probe track (aided by DiI) and optic fiber tracks.

For immunostaining, mice were deeply anesthetized with overdosed urethane and perfused transcardially by saline followed either by 4% PFA or by the Sloviter protocol [i.e., 2% (wt/vol) PFA in acetate buffer (pH 6.5) for 3 min followed by 2% (wt/vol) PFA in borate buffer (pH 8.5) for 40 min]. After perfusion brains were removed and stored in fixative solution overnight. Then, 50-μm sections were prepared on a vibrotome (Leica). Then, sections were washed in 0.1 M phosphate buffer (PB), cryoprotected overnight in 30% (wt/vol) sucrose dissolved in 0.1 M PB, and freeze-thawed in aluminum foil boats over liquid nitrogen to enhance penetration of the antisera. Next, after several changes of PB, the sections were transferred into Tris-buffered saline (TBS, pH 7.4). All of the following washes and antisera dilutions were carried out in TBS. Sections were incubated in primary antibody solution for two nights at 4 °C. Then, primary serum was washed, followed by incubation in secondary antibody solution for 3 h at room temperature, followed by extensive washing. Finally, sections were mounted on glass slides and covered by Vectashield.

Antibodies used were mouse monoclonal anti-ChAT primary (1:500; see ref. 6) and Alexa-647 conjugated donkey anti-mouse secondary (1:500) and chicken polyclonal anti-GFP primary (1:2,000; Life Technologies) and Alexa-488 conjugated goat anti-chicken secondary (1:500). In a subset of experiments, Rabbit polyclonal anti-parvalbumin (1:1,000; Swant) and Alexa 594-conjugated goat anti-rabbit secondary (1:500) were used. All secondaries were purchased from Life Technologies.

Sections were examined either by an A1R or C2 confocal laser scanning microscope (Nikon) or by an Axioplan-2 microscope (Zeiss). Photomicrographs were taken by the fluorescent detector of the A1R or C2 microscope, or by an Olympus DP-70 CCD camera (Olympus) on the Zeiss microscope. Adjustments of look-up tables of images were accomplished using Adobe Photoshop CS (Adobe Systems Inc.).

Data Analysis. Data were visualized and processed using NeuroScope and NDManager (7) (http://neurosuite.sourceforge.net) and analyzed by MATLAB (MathWorks) built-in or custom-built procedures. For unit detection in MS, single units were isolated from the wideband signal using the semiautomatic spike classifier KlustaKwik (http://sourceforge.net/projects/klustakwik) and further refined manually using the graphical spike sorting application Klusters (7) (http://neurosuite.sourceforge.net). Only units responding to light were analyzed. For analysis of the effect in hippocampus, mice with an optrode in the MS (four animals) are excluded from analysis, because the low light power emanating from the tip of the optrode would be unlikely to recruit a large and consistent enough population of cholinergic neurons to affect the hippocampus efficiently and reproducibly.

Mutlilayer Spectral Analysis. Only mice with linear probe recordings and a full optic fiber in the MS are included in multilayer analysis (10 anesthetized and 4 behaving mice). LFP signals were extracted from broadband signals by low-pass filtering at 1.25 kHz; malfunctioning channels were manually identified and excluded from analysis. The anatomical localization of each channel was then deduced from LFP features (ripples, sharp waves, and theta and gamma depth profile) as well as histological confirmation of the probe track, and five channels were chosen in each recording to represent the five layers analyzed: CA1 oriens, pyramidal, radiatum, stratum lacunosum-moleculare, and dentate gyrus (DG). DG sublayers were not distinguished because all were not similarly represented in all mice (in particular with 100-μm-spacing linear probes). Current source density (CSD) was calculated as the second spatial derivative of the LFP (8) with a 100-μm step. For CSD calculations, when needed, malfunctioning channels were replaced by the interpolation of the surrounding channels (in no case were there two contiguous bad channels). For each stimulation epoch, a control period of the same duration situated right before the stimulation period was defined. For each control and stimulation pair of epochs, the mean power and coherence spectrum of LFP and CSD signals were computed using multitaper Fourier analysis (9). When power ratios were used (theta/slow oscillation or low/medium gamma), the cumulative power over each band was normalized by the width of the band in hertz. The global dominant frequency of each epoch was taken as the frequency above 1 Hz with maximal power.

For theta-gamma phase-power coupling, LFP signal for each epoch was filtered at theta frequency (2–6 Hz for anesthesia, 4–10 Hz for drug-free) and at the chosen gamma subbands (20–40 or 40–80 Hz for anesthesia and 30–70 or 70–100 Hz for drug-free animals). Theta phase and gamma amplitude, respectively, were extracted using a Hilbert transform. The modulation index was computed using an adaptation of the Kullback–Leibler distance between the observed distribution and a uniform distribution, as described in ref. 10. The preferred phase was determined as the theta phase bin in which the maximal gamma power was observed.

For wavelet analysis, raw signal was down-sampled to 200 Hz to decrease computation load and then transformed by wavelet decomposition using a linear wavelet scale. Number of scales was 400 ranging from 0.5 to 100 Hz (minimum and maximum frequency in the decomposition). The continuous wavelet transform of the sampled time series *xn* is a convolution of it with the wavelet function Ψ:

$$W_n(s) = \sum_{n'=0}^{N-1} x_{n'} \Psi^{\star} \left[\frac{(n'-n)\delta t}{s} \right].$$

For the calculation of the wavelet power spectrum, the Morlet wavelet was used (11):

$$\Psi_0(\eta) = \pi^{-1/4} e^{i\omega_o \eta} e^{-\eta^2/2}.$$

For the wavelet decomposition the algorithm of Torrence and Compo was used (12). For each control and stimulation epoch we determined the theta-dominated LFP samples: time samples in which the dominant frequency (corresponding to the scale with maximal coefficient) was within theta band (2–6 Hz for anesthesia, 4–10 Hz for behaving). Theta proportion was calculated as the ratio of the number of theta-dominated samples over the total number of samples per epoch, and theta frequency as the median of the dominant frequencies of theta-dominated samples. Within each control and stimulation epoch theta segments were defined as segments composed of ≥100 (500 ms) contiguous theta-dominated samples. For state dependence, trials were segregated into two categories based on the presence of ripples and on the dominant frequency in the control epoch: "ripple trials" were characterized by the presence of at least one ripple in the control epoch, and "theta-dominant trials" by the absence of ripple in the control epoch together with the control epoch dominant frequency (from Fourier analysis) within theta range (2–6 Hz for anesthesia, 4–10 Hz for behaving).

Ripple Analysis. For ripple detection, the 1.25-kHz down-sampled LFP signal in the pyramidal layer channel was band-pass-filtered (80–250 Hz) and ripple epochs were defined as periods during which ripple-band power was greater than mean +2 SD, with a peak power >4 SD and a minimum duration of 40 ms. Thresholds were adjusted if needed after visual inspection of each recording. Sessions where no ripples were detected in the entire recording time were excluded from the ripple analysis (such as isoflurane anesthesia recordings). In the remaining sessions (from nine mice under urethane anesthesia, including three control mice, and eight behaving mice) all trials were included, independently of the presence or absence of ripples in each individual control epoch. The occurrence of ripples was then calculated for each mouse as the overall number of ripples in all control/stimulation periods divided by the overall duration of control/stimulation epochs.

Statistics. Unless otherwise stated, data are reported as medians and 25–75% quartiles, and statistical significance was computed using nonparametric paired tests when comparing control and stimulation epoch pairs (Wilcoxon's signed rank test). Bonferroni's correction for multiple testing was used when testing for five layers or 10 layer pairs. Statistics were computed using MATLAB or Prism (GraphPad Software). For circular data (preferred theta phase for theta–gamma coupling), the statistics were calculated using the Circular Statistics Toolbox for MATLAB (13). Data are presented as circular mean and distribution, and statistical testing of stimulation effect (control vs. stimulation epoch pairs) is computed by testing the median of the stimulation–control circular distance against 0 with a binomial test.

1. Madisen L, et al. (2012) A toolbox of Cre-dependent optogenetic transgenic mice for light-induced activation and silencing. *Nat Neurosci* 15(5):793–802.
2. Vandecasteele M, et al. (2012) Large-scale recording of neurons by movable silicon probes in behaving rodents. *J Vis Exp* 61(61):e3568.
3. Stark E, Koos T, Buzsáki G (2012) Diode probes for spatiotemporal optical control of multiple neurons in freely moving animals. *J Neurophysiol* 108(1):349–363.
4. Royer S, et al. (2010) Multi-array silicon probes with integrated optical fibers: Light-assisted perturbation and recording of local neural circuits in the behaving animal. *Eur J Neurosci* 31(12):2279–2291.
5. Berényi A, et al. (2014) Large-scale, high-density (up to 512 channels) recording of local circuits in behaving animals. *J Neurophysiol* 111(5):1132–1149.
6. Umbriaco D, Watkins KC, Descarries L, Cozzari C, Hartman BK (1994) Ultrastructural and morphometric features of the acetylcholine innervation in adult rat parietal cortex: An electron microscopic study in serial sections. *J Comp Neurol* 348(3):351–373.
7. Hazan L, Zugaro M, Buzsáki G (2006) Klusters, NeuroScope, NDManager: A free software suite for neurophysiological data processing and visualization. *J Neurosci Methods* 155(2):207–216.
8. Mitzdorf U (1985) Current source-density method and application in cat cerebral cortex: Investigation of evoked potentials and EEG phenomena. *Physiol Rev* 65(1):37–100.
9. Mitra PP, Pesaran B (1999) Analysis of dynamic brain imaging data. *Biophys J* 76(2):691–708.
10. Tort ABL, et al. (2008) Dynamic cross-frequency couplings of local field potential oscillations in rat striatum and hippocampus during performance of a T-maze task. *Proc Natl Acad Sci USA* 105(51):20517–20522.
11. Muthuswamy J, Thakor NV (1998) Spectral analysis methods for neurological signals. *J Neurosci Methods* 83(1):1–14.
12. Torrence C, Compo GP (1998) A practical guide to wavelet analysis. *Bull Amer Meteor Soc* 79(1):61–78.
13. Berens P (2009) CircStat: A MATLAB toolbox for circular statistics. *J Stat Softw* 31:10.

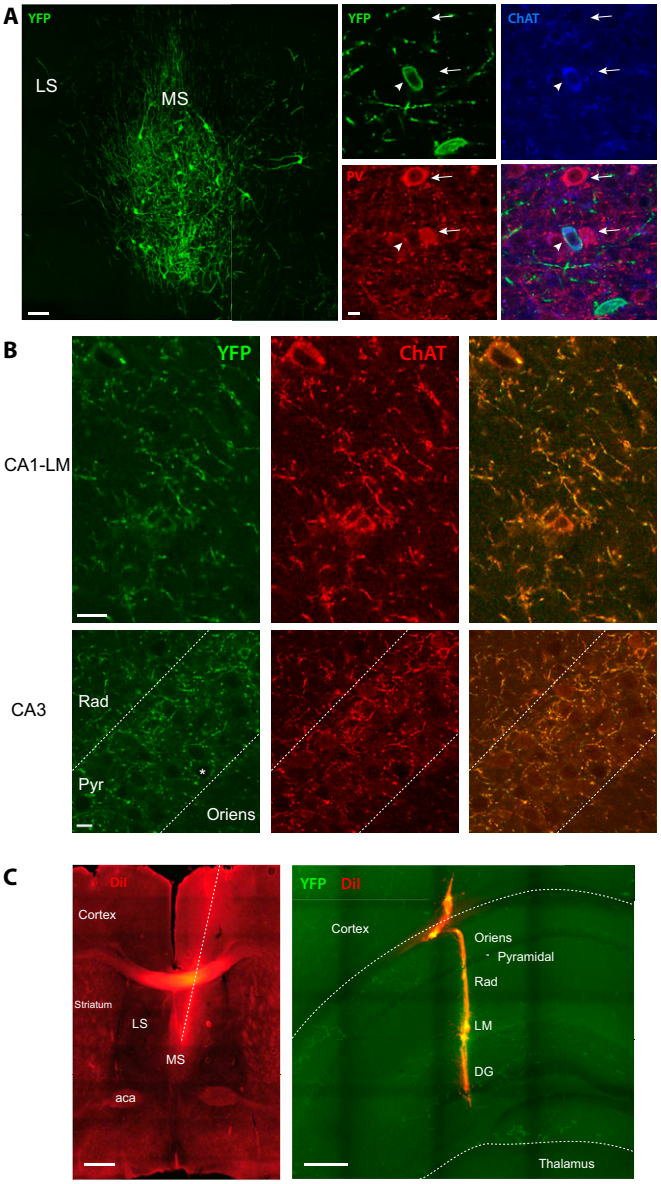

Fig. S1. (*A*) Left-most panel: YFP immunostaining in the MS of a ChAT-cre mouse injected with cre-dependent ChR2-YFP virus. (Scale bar: 100 μm.) Right panels: MS cells at higher magnification, showing the specific expression of YFP in ChAT neurons by triple immunostaining for YFP (green), ChAT (blue), and parvalbumin (red). Arrowhead: YFP-positive, ChAT-positive, and parvalbumin-negative cell body. Arrows: YFP-negative, ChAT-negative, and parvalbumin-positive cell bodies. (Scale bar: 10 μm.) (*B*) YFP- (green) and ChAT-positive (red) fibers in the CA1 stratum lacunosum-moleculare (*Upper*) and CA3 pyramidal layer (*Lower*). Asterisk indicates a putative pyramidal cell soma. (Scale bars: 10 μm.) (*C*) (*Left*) Optrode track (dotted line), revealed by DiI staining in a mouse with optogenetically entrained putative ChAT neurons in the MS. (Scale bar: 500 μm.) (*Right*) DiI-labeled track of hippocampal silicon probe spanning CA1 and DG regions. (Scale bar: 200 μm.) aca, anterior commissure; DG, dentate gyrus; LM, stratum lacunosum-moleculare; LS, lateral septum; MS, medial septum; PV, parvalbumin; Pyr, stratum pyramidale; Rad, stratum radiatum.

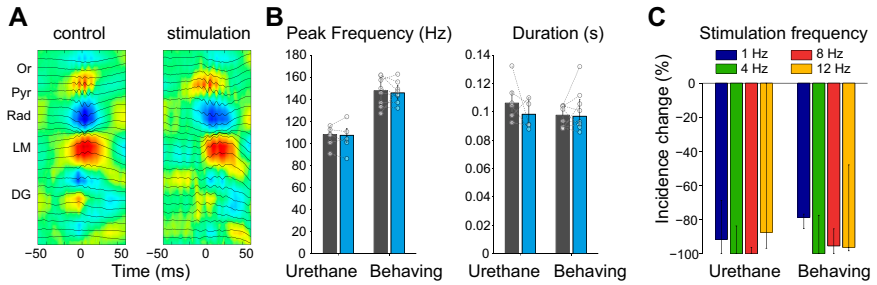

Fig. S2. (*A*) Sharp wave ripples detected in control (*Left*, triggered average of $n = 31$ ripple events) or during stimulation (*Right*, $n = 2$ ripple events) have similar LFP (black lines) and CSD (sources in red, sinks in blue). (*B*) The peak frequency (*Left*) and duration (*Right*) of ripples are unchanged during stimulation in all mice in both urethane anesthesia ($n = 6$ mice) and freely moving conditions ($n = 8$ mice). Bars/error bars are medians and quartiles for all animals, and paired dots represent individual mice. (*C*) Although the magnitude of suppression seemed less efficient for sinusoidal stimulations at 1 Hz than at higher frequencies (median and quartiles, all animals pooled), the frequency dependence was not significant (repeated-measures ANOVA, $P > 0.1$ in both conditions).

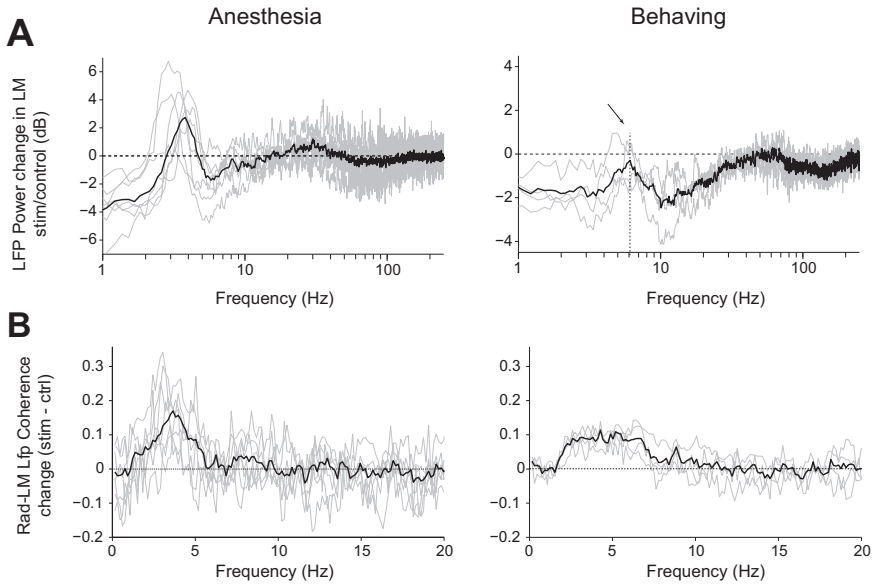

Fig. S3. Stimulation effects on LFP power in LM (*A*) and Rad-LM coherence (*B*) in each individual animal (thin gray lines) with the median across animals (thick black line).

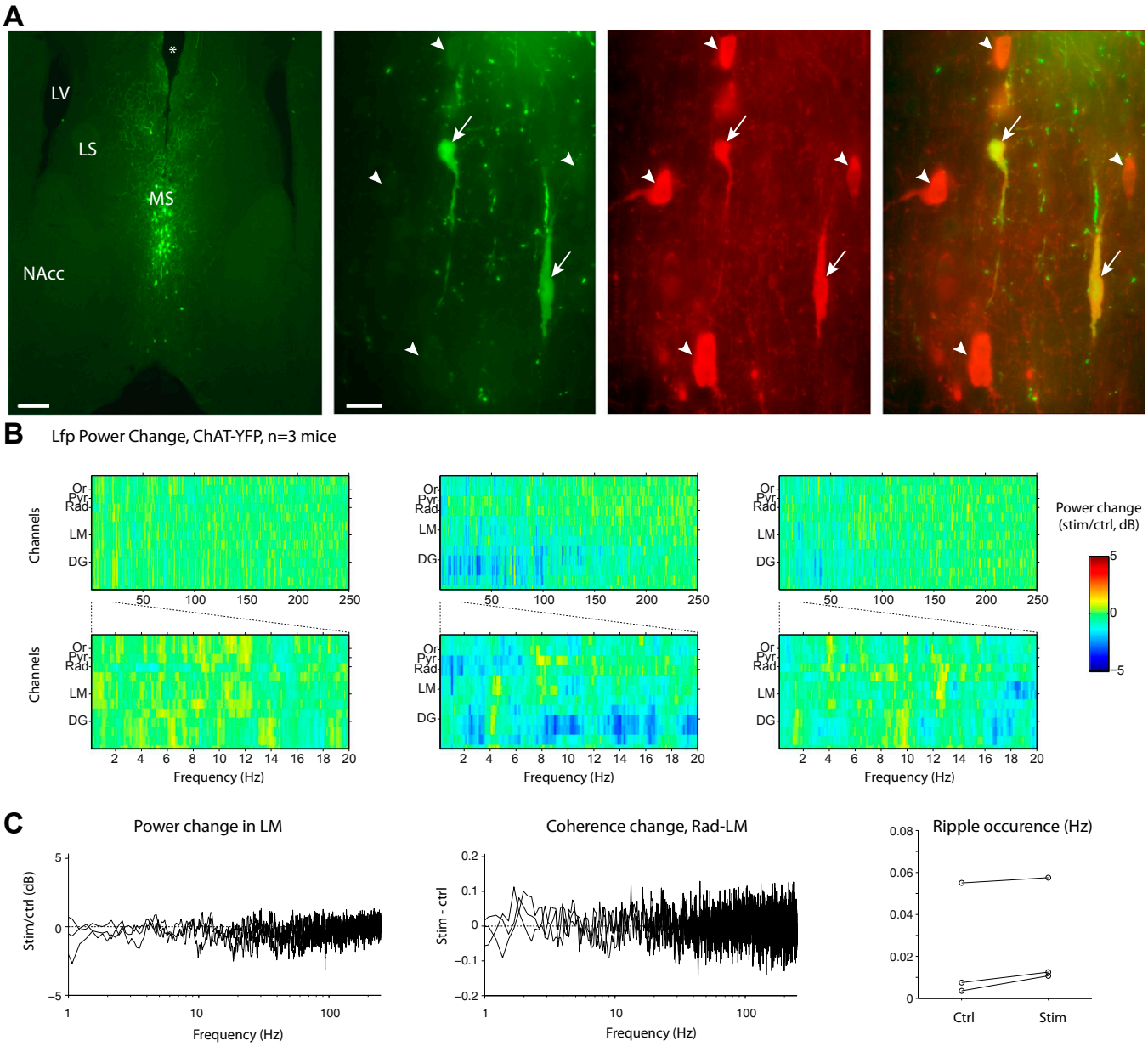

Fig. S4. Optogenetic stimulation of MS in urethane-anesthetized ChAT-YFP animals does not affect hippocampal activity. (*A*) Specific expression of YFP in ChAT neurons, as revealed by double immunostaining for ChAT (red) and YFP (green). Left-most panel: ChAT-cre mouse injected with YFP-only virus, showing YFP expression in the MS at low magnification. Asterisk indicates injection cannula and optic fiber track. (Scale bar: 200 μm.) Right panels: MS of the same mouse at higher magnification, showing the specific expression of the YFP in ChAT-positive neurons (arrows). Arrowheads are YFP-negative ChAT neurons. LS, lateral septum; LV, lateral ventricle; MS, medial septum; NAcc, nucleus accumbens. (Scale bar: 20 μm.) (*B*) Optogenetic stimulation of the MS (10-s-long sine wave at 1, 4, 8, or 12 Hz, median of 40 trials, maximum power output 9.4 mW) triggers no visible effect on the hippocampal LFP in urethane-anesthetized mice expressing YFP-only in ChAT neurons ($n = 3$ animals, each column is a different mouse). Recording sites are linearly arranged with 100-μm spacing. (*C*) Optogenetic stimulation in urethane-anesthetized ChAT-YFP mice fails to trigger three main effects observed in ChAT-ChR2-YFP animals: No change is observable in LFP power in stratum lacunosum-molecular (LM, *Left*) or in Rad-LM coherence (*Center*). Optogenetic stimulation had no effect on ripple occurrence either (*Right*).

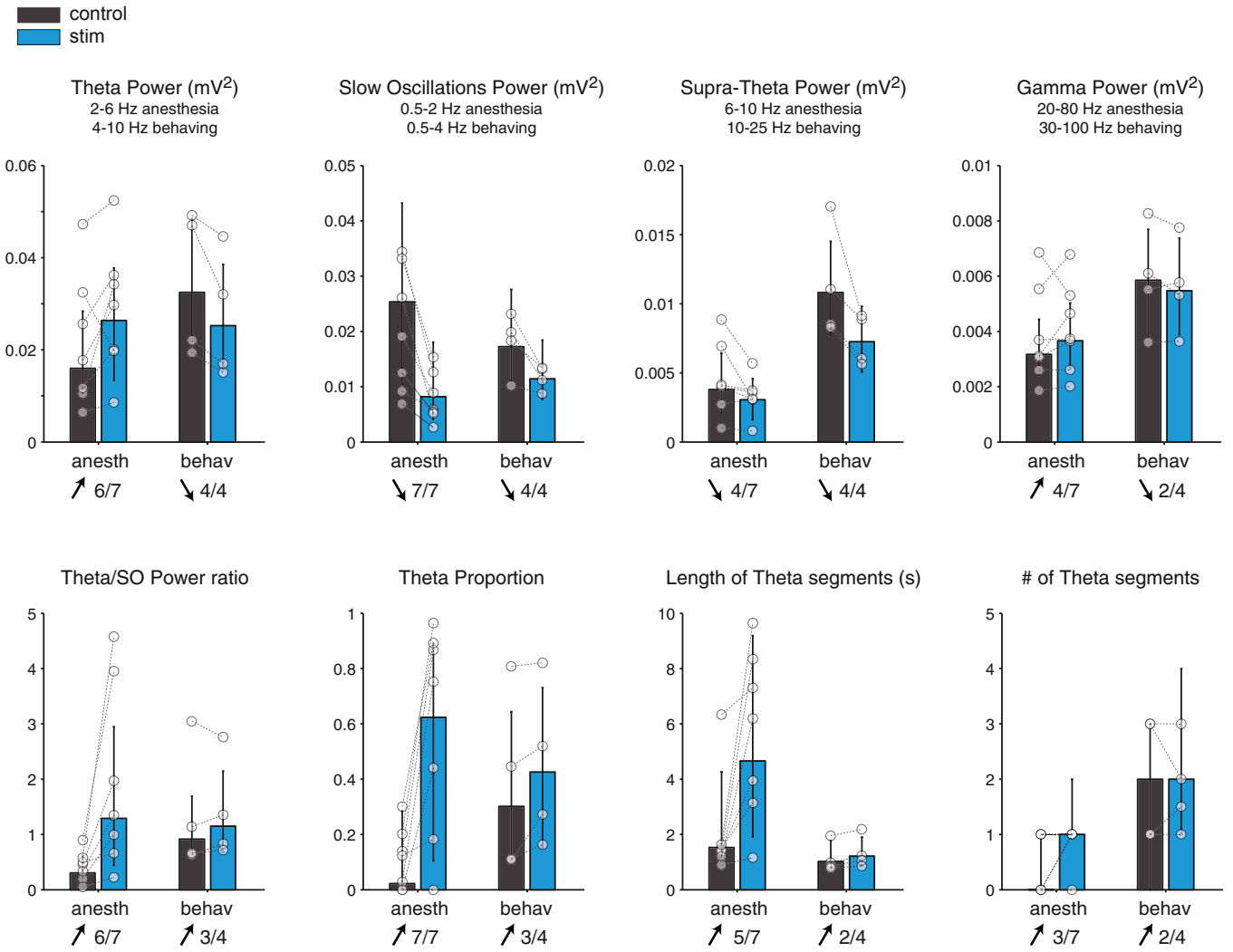

Fig. S5. Quantification of hippocampal LFP power changes induced by MS stimulation (10-s sinusoidal stimulation, 1–12 Hz). Bars represent the median and quartiles of all mice (all trials pooled); paired dots represent each animal; numbers below each condition indicate the proportion of animals displaying an individually significant change in the indicated direction.

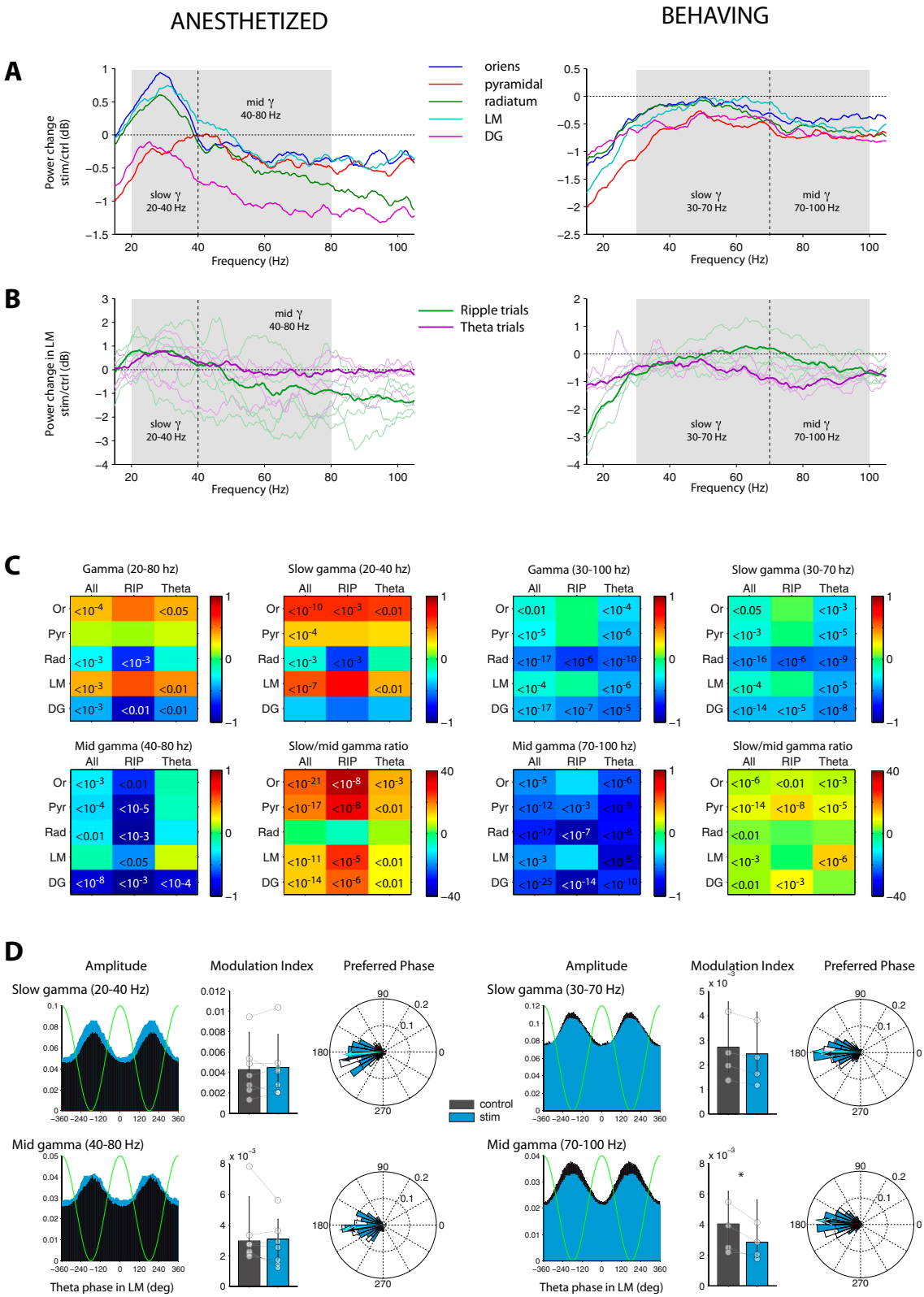

Fig. S6. Effect of MS stimulation on hippocampal gamma power and theta–gamma coupling in anesthetized (left column) and behaving (right column) mice. (*A*) LFP power changes in the gamma band in different layers (median power change, all trials pooled, $n = 296$ trials from seven anesthetized mice, $n = 417$ trials from four behaving animals). (*B*) LFP gamma power change in stratum lacunosum-moleculare (LM), segregated according to the brain state during the control epoch. The thick line represents the median across all trials ($n = 69$ and $n = 84$ for ripple and theta trials, respectively, under anesthesia, $n = 165$ and $n = 159$ in drug-free); thin lines correspond to individual animals. (*C*) Comparison of gamma change induced by optogenetic stimulation of the MS in five hippocampal layers, in all trials, ripple trials (RIP), and theta trials. For each condition, the three top-left, top-right, and bottom-left color plots represent gamma power change in the entire gamma band, slow gamma band, and mid-gamma band, respectively (median change across trials, decibels). The bottom right color

Legend continued on following page

plot represents the change (in percent of control) in the ratio of slow/mid-gamma power. In each color plot the color indicates the median change; number indicates the *P* value for the significant changes (Wilcoxon's rank sum test with Bonferroni correction for five layers). (*D*) Comparison of theta–gamma coupling in LM during control (black) and stimulation (blue) epochs for each gamma subband (slow gamma: *Upper*; mid-gamma: *Lower*) in anesthetized (left column) and behaving (right column) animals. The amplitude of gamma was plotted against theta phase (*Left*). From this distribution, the modulation index (*Center*) and the preferred phase (*Right*) were computed and compared in control and stimulation epochs. $*P < 0.05$ (Wilcoxon's rank sum test with Bonferroni correction for five layers). The decrease in LM modulation index was not significant when individual animals were considered. Note that the differential changes in the gamma-band of anesthetized and waking mice are reminiscent of the changes observed in theta band (see Fig. 3).

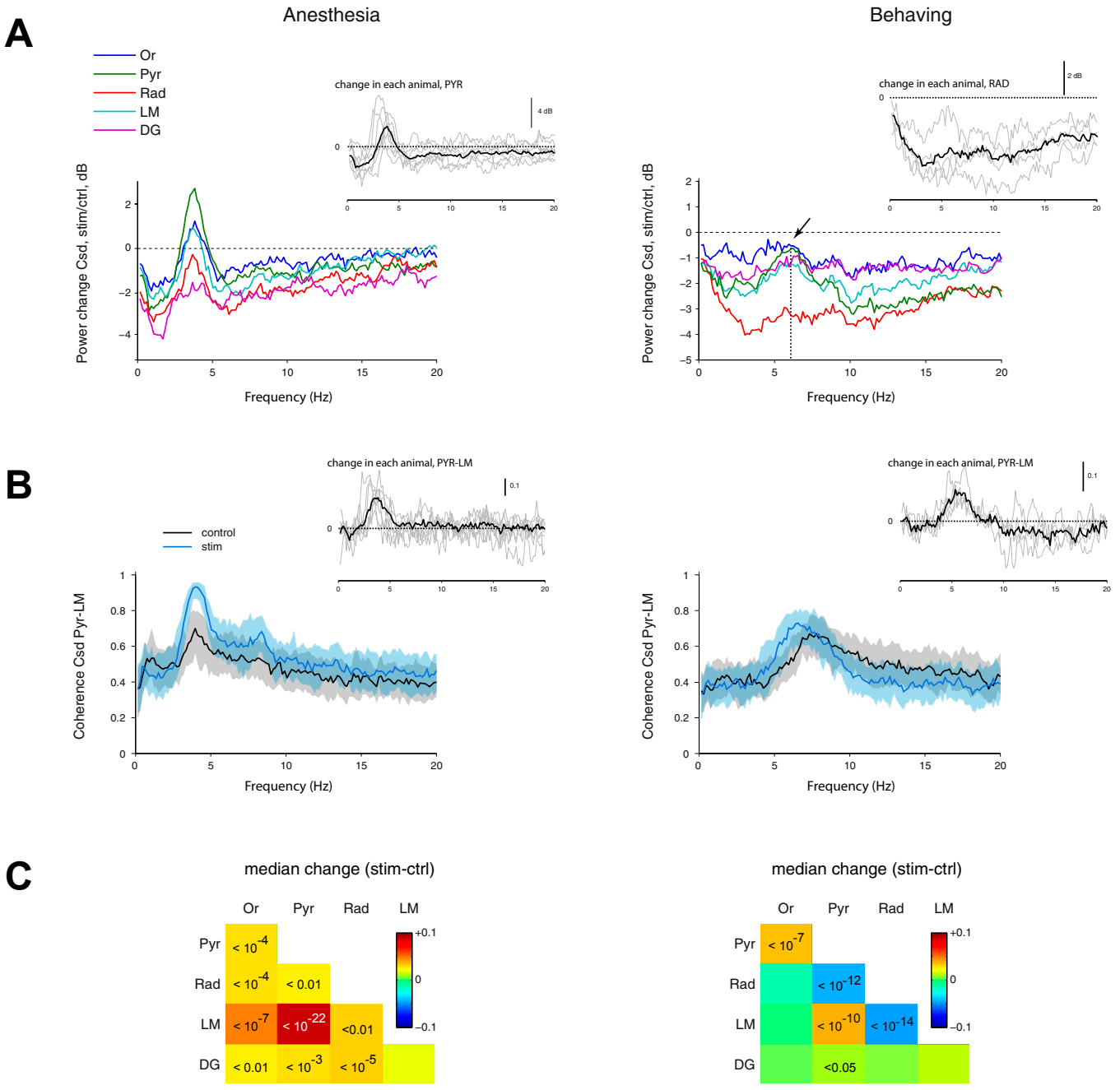

Fig. S7. Effect of MS stimulation on hippocampal CSD power and coherence in anesthetized (left column) and behaving (right column) mice. (*A*) CSD power changes in different layers (all trials pooled). Arrow and vertical line indicate the spared theta frequency in Pyr layer for behaving animals. (*Insets*) Change in the most affected layer (thick line, group; thin lines, individual animals): Pyr in anesthesia: median CSD power change in theta band +1.4 dB ($P < 10^{-24}$, $n = 296$ trials, individually significant in six out of seven mice), and Rad in behaving mice: median CSD power change in theta band −2.7dB ($P < 10^{-45}$, $n = 417$ trials, individually significant in four of four mice). Note that the effect on Rad CSD in behaving animals is two- to fivefold stronger than in other layers, whereas the effect in LFP power was in the same range across layers (see Fig. 3*C*). (*B*) CSD coherence between Pyr and LM in control (black) and stimulation (blue) epochs, median of all trials in representative animals ($n = 98$ in an anesthetized animal, $n = 82$ in a behaving animal; interquartile area is shaded). (*Insets*) Pyr-LM coherence change in all animals (thick lines), and each individual animal (thin lines). (*C*) CSD coherence change in theta band for each hippocampal layer pair. In each square, the color indicates the median change (all trials pooled); the number indicates the *P* value for the significant changes (Wilcoxon's rank sum test, with Bonferroni's correction for 10 layer pairs).

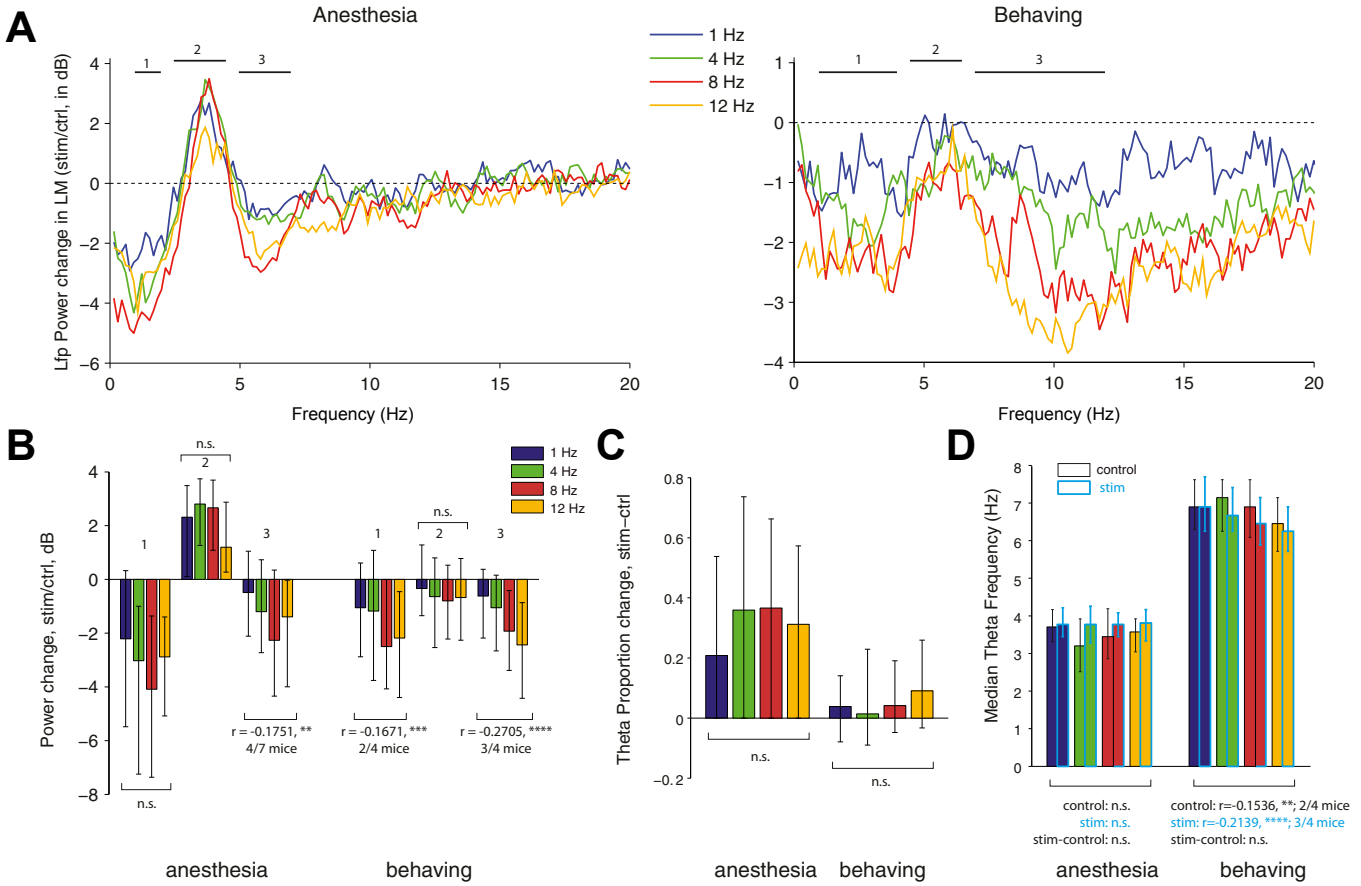

Fig. S8. Effect of stimulation frequency. (*A*) LFP power changes induced by MS stimulation at 1, 4, 8, and 12 Hz (median of all trials, $n = 73$, 80, 73, and 70, respectively, for anesthetized trials; $n = 94$, 135, 96, and 92, respectively, for behaving trials). Numbered horizontal lines represent the subbands quantified in *B*. (*B*) Power changes in each spectrum subband: Subbands 1 (slow oscillation) and 3 (supratheta band) are significantly more affected at higher stimulation frequencies, whereas theta band (subband 2) is not. Significant correlations of stimulation frequency with the effect on each subband are indicated (Spearman's rho, $*P < 0.05$, $***P < 0.001$, $****P < 0.0001$; the number of animals in which the correlation is individually significant is indicated). (*C*) Theta proportion change displays a nonsignificant increase with stimulation frequency. (*D*) Theta frequency in theta-dominated samples in control (black outline) and stimulation (cyan outline) epochs. Significant correlations of stimulation frequency with theta frequency in control, with theta frequency during stimulation, and with the effect on theta frequency are indicated (spearman's rho, $**P < 0.01$, $****P < 0.0001$; the number of animals in which the correlation is individually significant is indicated). We assume that higher frequency stimulation induced more spikes per unit time in the MS cholinergic neurons, and therefore enhanced the release of the amount of acetylcholine. The slight tendency that 4- and 8-Hz stimulation exerted the maximum effects in anesthetized preparation warrants further investigation, however.

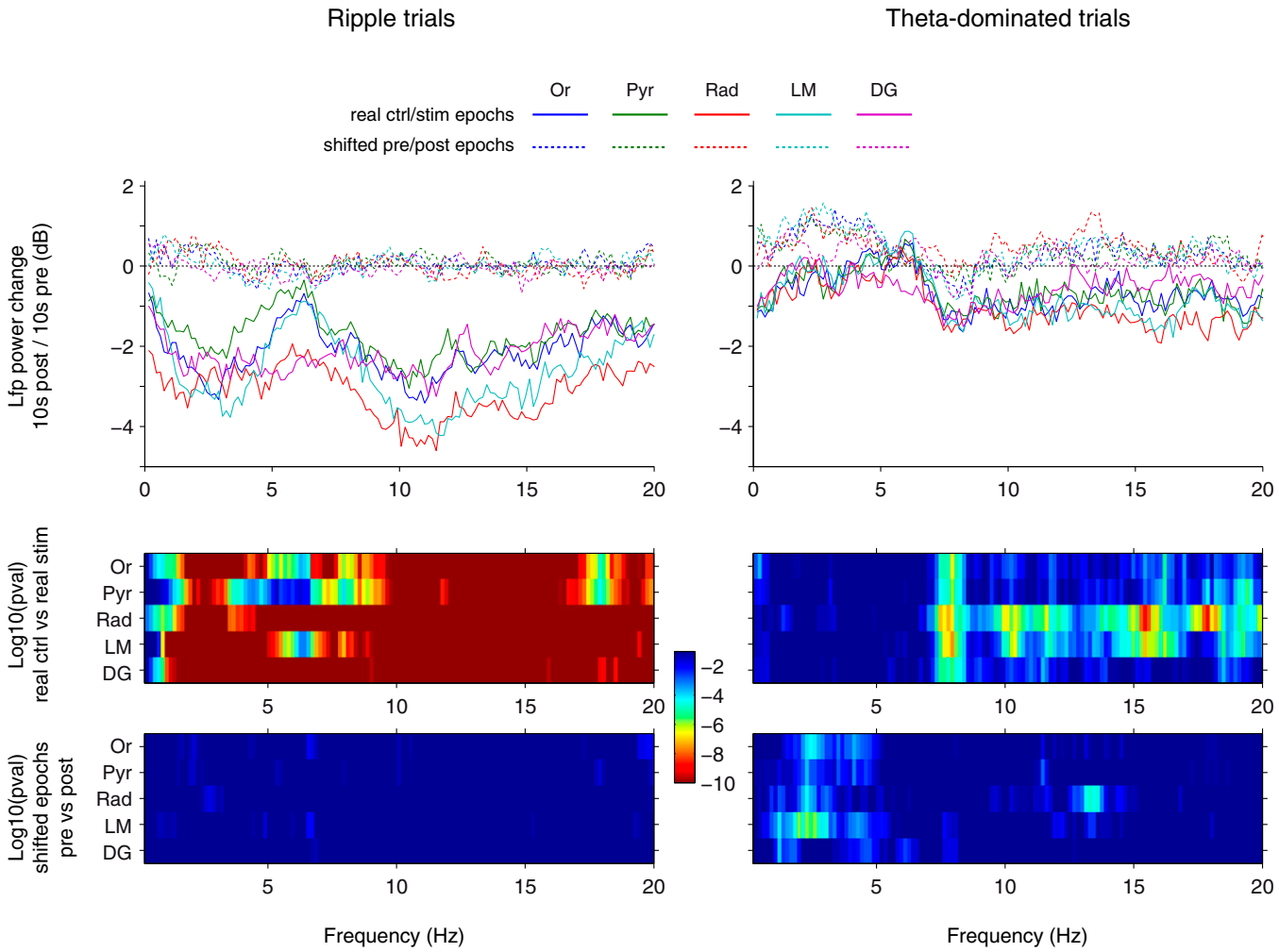

Fig. S9. Shift analysis of trial segregation effect in behaving mice. Comparison of two 10-s-long epochs starting at 10 s and 20 s before MS stimulation. (*A*) LFP power changes in all hippocampal layers for real control/stimulation epoch pairs (continuous lines) and shifted pre/post epoch pairs (dotted lines). (*B*) Color plots of significance (log of *P* values computed from Wilcoxon's rank sum test), computed for real control/stimulation epoch pairs (*Upper*) and for shifted pre/post epoch pairs (*Lower*) for each frequency bin in each layer.